Comparison of Quantitative Perfusion Imaging Using Arterial Spin Labeling at 1.5 and 4.0 Tesla

Jiongjiong Wang,[1,2] David C. Alsop,[5] Lin Li,[4] John Listerud,[3] Julio B. Gonzalez-At,[2] Mitchell D. Schnall,[1] and John A. Detre[1,2*]

High-field arterial spin labeling (ASL) perfusion MRI is appealing because it provides not only increased signal-to-noise ratio (SNR), but also advantages in terms of labeling due to the increased relaxation time T_1 of labeled blood. In the present study, we provide a theoretical framework for the dependence of the ASL signal on the static field strength, followed by experimental validation in which a multislice pulsed ASL (PASL) technique was carried out at 4T and compared with PASL and continuous ASL (CASL) techniques at 1.5T, both in the resting state and during motor activation. The resting-state data showed an SNR ratio of 2.3:1.4:1 in the gray matter and a contrast-to-noise ratio (CNR) of 2.7:1.1:1 between the gray and white matter for the difference perfusion images acquired using 4T PASL, 1.5T CASL, and 1.5T PASL, respectively. However, the functional data acquired using 4T PASL did not show significantly improved sensitivity to motor cortex activation compared with the 1.5T functional data, with reduced fractional perfusion signal change and increased intersubject variability. Possible reasons for these experimental results, including susceptibility effects and physiological noise, are discussed. Magn Reson Med 48:242–254, 2002. © 2002 Wiley-Liss, Inc.

Key words: arterial spin labeling (ASL); cerebral blood flow (CBF); magnetic field strength; multislice perfusion fMRI; susceptibility effect

The past decade has seen the emergence of arterial spin labeling (ASL) perfusion MRI (1,2) and its development into a class of noninvasive methods for direct measurement of cerebral blood flow (CBF) (3–11). ASL perfusion MRI uses magnetically labeled arterial blood water as an endogenous tracer for measuring CBF, and is less invasive and less expensive than earlier approaches using radioactive tracers or paramagnetic contrast agents. In clinical applications, ASL has been demonstrated to provide reproducible and reliable quantitative CBF measurements in the presence of various cerebrovascular disorders in the brain (12–14). The repeatability and high temporal resolution of the ASL perfusion technique also makes it suitable for functional MRI (fMRI) studies. Compared with blood oxygenation level dependent (BOLD) fMRI, ASL-based fMRI has certain advantages, particularly for clinically related studies. First, ASL perfusion MRI provides absolute quantification of a well-characterized physiological parameter, while the BOLD signal is the result of complex interactions between CBF, cerebral blood volume, and oxygen consumption. Second, the ASL method is less susceptible to baseline drift and motion artifact, and is likely to be preferable for imaging slow variations in regional brain activity such as behavior state change and pharmacological interventions (4,15). Furthermore, the ASL contrast is not based on susceptibility effects and could be used to study brain activation in regions of high static field inhomogeneity, such as the orbital frontal cortex and inferior temporal lobe (16–18). ASL perfusion MRI may become the method of choice for a wide range of clinical applications of both resting brain function and regional activation.

There are, however, several disadvantages of the current ASL techniques which have delayed their widespread application. One primary limitation is the relatively low signal-to-noise ratio (SNR). Due to the small fractional effect of labeling on imaging intensity (<1% raw signal) (3,4), ASL perfusion images can be of poor image quality even after lengthy signal averaging, resulting in reduced diagnostic reliability and sensitivity to brain activity with the ASL technique. Another limitation is the relatively short signal decay rate. In humans, the arterial transit time for the flow of blood from the tagged region to the imaging slices is comparable with the T_1 of blood (3,4). As a result, the amount of spin labeling is greatly reduced by the time it reaches brain tissue, leading to further difficulty in perfusion signal detection, and the potential for errors in perfusion quantification due to uncertainties in transit time. In addition, some of the existing ASL techniques are unable to provide satisfactory imaging coverage because T_1 limits the time available for multislice acquisition before the label decays.

One natural solution for circumventing these limitations is to implement the ASL technique at high field. High-field ASL would provide not only increased SNR that is proportional to the main field strength, but also an important advantage for labeling. Because of the increase in the relaxation time T_1 at high field, the loss of spin labeling during the transit time is decreased and the accumulation of labeled spins is increased as compared to 1.5 T, producing greater perfusion signal in brain tissue while reducing the arterial transit-related artifacts and quantification errors. This T_1 effect, in combination with the increased SNR, could yield major improvements in the perfusion signal, allowing increased spatial and temporal resolution

[1]Department of Radiology, University of Pennsylvania, Philadelphia, Pennsylvania.

[2]Department of Neurology, University of Pennsylvania, Philadelphia, Pennsylvania.

[3]Department of Psychiatry, University of Pennsylvania, Philadelphia, Pennsylvania.

[4]Department of Metabolic Magnetic Resonance Research and Computing Center, Department of Radiology, University of Pennsylvania, Philadelphia, Pennsylvania.

[5]Department of Radiology, Beth Israel Deaconess Medical Center, Harvard Medical School, Boston, Massachusetts.

Grant sponsor: NIH; Grant numbers: HD39621; AG19599; Grant sponsor: GE Medical Systems.

*Correspondence to: John A. Detre, M.D., Department of Neurology, University of Pennsylvania, 3400 Spruce St., Philadelphia, PA 19104.
E-mail: detre@mail.med.upenn.edu

Received 30 October 2001; revised 15 February 2002; accepted 7 March 2002.

DOI 10.1002/mrm.10211

Published online in Wiley InterScience (www.interscience.wiley.com).

as well as wider imaging coverage. In the present study, the feasibility of high-field quantitative perfusion imaging was demonstrated by carrying out pulsed ASL (PASL) at 4T. One challenge for high-field ASL is the high specific absorption rate (SAR) of the labeling pulse. PASL techniques use nearly instant radiofrequency (RF) pulses for spin labeling, and are particularly advantageous at high field because of relatively low levels of RF deposition (4). Continuous ASL (CASL) can also be implemented at high field with a special multicoil approach (19) or a single-coil approach with simultaneous modulation of the RF and gradient for labeling (20).

In recent years, various studies have been carried out at high field using the PASL (7,21) or CASL (19,20) technique. However, the dependence of the ASL perfusion signal on the static field strength has not been systematically addressed. In this study, we calculate the theoretical ASL perfusion signal as a function of field strength, and report our results from direct experimental comparison of the resting state and activation perfusion images acquired on normal human brain using 4T PASL, 1.5T CASL, and 1.5T PASL.

THEORY

In order to minimize the transit time artifacts, Alsop and Detre (10) suggested introducing a delay between the end of the labeling pulse and image acquisition in CASL. This delay time, w, ideally should be greater than the transit time from the tagging region to the arterial vascular compartment, δ_a, allowing the delivery of all the tagged blood into the imaging slices. Once this assumption is satisfied, the transit time error can be greatly reduced since there is only a small difference between the T_1's of blood and brain tissue. According to the two compartment perfusion model proposed by Alsop and Detre (10), and taking into account the tagging duration, τ, the CASL difference signal (tag-control), ΔM, can be expressed by the following equation (see Appendix)

$$\Delta M = \frac{-2M_0 f\alpha}{\lambda}\begin{cases}\dfrac{\exp(-\delta R_{1a})}{R_{1app}}[\exp(\min(\delta - w,0)R_{1app}) - \exp((\delta - \tau - w)R_{1app})] + \\ \dfrac{1}{R_{1a}}[\exp((\min(\delta_a - w,0) - \delta_a)R_{1a}) - \exp((\min(\delta - w,0) - \delta)R_{1a})\ ]\end{cases} \quad \tau + w > \delta$$

$$\Delta M = \frac{-2M_0 f\alpha}{\lambda R_{1a}}[\exp((\min(\delta_a - w,0) - \delta_a)R_{1a}) - \exp(-(\tau + w)R_{1a})] \quad \tau + w < \delta \qquad [1]$$

where M_0 is the equilibrium brain tissue magnetization; f is CBF; λ is the blood/tissue water partition coefficient; R_{1a} is the longitudinal relaxation rate of blood; α is the inversion efficiency; $R_{1app} = R_1 + f/\lambda$, R_1 is the longitudinal relaxation rate of brain tissue in the absence of blood flow; δ is the transit time from the labeling region to the tissue compartment (exchange time); and the min( ) function returns the smaller of its two arguments. In the presence of the magnetization transfer (MT) effect and $\tau + w > \delta$, ΔM is given by

$$\Delta M = \frac{-2M_0 f\alpha}{\lambda}\begin{cases}\dfrac{\exp(-\delta R_{1a})}{R_{1ns}}[\exp(\min(\delta - w,0)R_{1ns}) - \exp(-wR_{1ns})] + \\ \dfrac{\exp(-\delta R_{1a})}{R_{1s}}\exp(-wR_{1ns})[1 - \exp(\min(\delta - \tau,0)R_{1s})] + \\ \dfrac{1}{R_{1a}}[\exp((\min(\delta_a - w,0) - \delta_a)R_{1a}) - \exp((\min(\delta - w,0) - \delta)R_{1a})]\end{cases} \qquad [2]$$

where R_{1s} and R_{1ns} are the longitudinal relaxation rates of brain tissue with and without off-resonance RF saturation, respectively.

An analogous approach was carried out by Wong et al. (11) in PASL. As proposed in quantitative imaging of perfusion using a single subtraction (QUIPSS II), a saturation pulse is applied at a time, TI_1, after the inversion pulse to externally define the tagging bolus duration, and images are acquired at a later time, TI_2. The delay time ($\Delta TI = TI_2 - TI_1$) should be greater than δ_a in order to minimize the effects of transit time and intravascular tagged blood. The PASL difference signal is given by the following equation

$$\Delta M = \frac{-2M_0 f\alpha}{\lambda}\begin{Bmatrix}\exp(-TI_2 R_{1app})[\exp(\min(TI_2,\delta + TI_1)\Delta R) - \exp(\delta\Delta R)]/\Delta R + \\ \exp(-TI_2 R_{1a})[(\min(\delta_a - \Delta TI,0) - \delta_a) - (\min(\delta - \Delta TI,0) - \delta)]\end{Bmatrix} \quad TI_2 > \delta$$

$$\Delta M = \frac{-2M_0 f\alpha}{\lambda}\exp(-TI_2 R_{1a})[\min(\delta_a - \Delta TI,0) - (\delta_a - TI_2)] \quad TI_2 < \delta \qquad [3]$$

where $\Delta R = R_{1app} - R_{1a}$. Note that when ΔTI or w is greater than δ_a, all of the above equations are insensitive to δ_a.

METHODS

Imaging Sequences

In this study, three ASL approaches were carried out for comparison: 4T PASL, 1.5T CASL, and 1.5T PASL. For PASL at 1.5 and 4T, we used a modified version of the flow-sensitive alternating inversion recovery (FAIR) technique (7), in which a saturation pulse was applied at TI_1 after the global or slice-selective inversion, similar to QUIPSS II. A slice-selective inversion pulse (frequency offset corrected inversion (FOCI) 16 ms, BW 10k) (22) was applied during tag, while the same pulse was used in the absence of gradients for global inversion during control. The slab of the slice-selective inversion was 2 cm thicker than the imaging slab, leaving a pair of 1-cm margins at each edge of the imaging slices to ensure optimum inversion. The saturation pulse was applied to a 10-cm slab inferior to the imaging slices with a 1-cm gap between the adjacent edges of the saturation and imaging slabs, and TI_1 was set to 800 ms according to Wong et al. (23). Interleaved tag and control images were taken using a gradient-echo echo planar imaging (EPI) sequence at TI_2 after the inversion pulse, followed by a recovery time to allow the arterial blood to be refreshed. The paradigm of the PASL sequence has been previously used in the FAIR exempting separate T_1 measurement technique (FAIREST) (24). The SAR of the 4T PASL sequence is below the FDA limit of 8 W/kg in a gram of tissue.

For CASL at 1.5T, we followed the original technique developed by Alsop and Detre (10,25). CASL was performed with a 0.25 G/cm gradient and 35 mG RF irradiation applied 8 cm beneath the center of the acquired slices. Interleaved images with (tag) and without (control) labeling were acquired using the same EPI sequence as in the PASL sequences. Controlling for off-resonance artifacts was effected by applying an amplitude modulated version of the labeling pulse. A postlabeling delay was inserted between the end of the labeling pulse and image acquisition. The tagging duration, τ, was about 2 s. According to Wong et al. (23), the labeling parameters used in our CASL and PASL sequences would yield optimal results in terms of SNR and imaging efficiency.

Resting-State Imaging

Imaging was performed on 1.5 and 4T whole-body scanners (GE Medical Systems, Milwaukee, WI), with the standard clinical quadrature head coils provided by the manufacturer. Except for the field strength and the use of an up/down converter to shift the resonant frequency, the 4T scanner is identical in design to the 1.5T scanner. Written informed consent was obtained prior to all human studies, and approval was obtained from the Institutional Review Board. Steady-state perfusion imaging was performed on five healthy male subjects (30–42 years old, mean age 36.6 years) at both 1.5 and 4T. As stated above, the same single-shot blipped gradient-echo EPI sequence was used for image acquisition for 4T PASL, 1.5T CASL, and 1.5T PASL. Acquisition parameters were: FOV = 24 cm × 16 cm, matrix = 64 × 40, TE = 23 ms, bandwidth = 62.5 kHz, slice thickness = 8 mm, interslice space = 2 mm. Eight slices were acquired from inferior to superior in an interleaved order, and each slice acquisition took about 60 ms. An inversion-prepared 3D spoiled GRASS sequence (TR/TE/TI = 33/7/400 ms, 256 × 192, 124 slices, 1.5 mm thick) was used to acquire high-resolution anatomical images for normalization and gray/white matter segmentation.

A preliminary experiment was carried out on two subjects at 4T to determine the appropriate ΔTI value for eight-slice imaging coverage by running the 4T PASL sequence at 5 ΔTI values (100, 400, 700, 1000, and 1500 ms). A ΔTI of ≥1000 ms was found to successfully suppress most of the intravascular signal in the ASL difference images (see Results). Therefore, two ΔTI values (1000 and 1500 ms) were used for PASL at both 1.5T and 4T with TR = 3.4 s. The same ΔTI values were applied for CASL at 1.5T with TR = 4s based on previous tests on normal subjects (26). For each scan of postlabeling delay, 90 acquisitions were carried out with a total scan time of 6 min and 5.1 min for CASL and PASL, respectively. "Dummy" gradient and RF pulses preceded each scan to allow tissue to reach steady-state magnetization.

Functional Activation Study

fMRI experiments with sensorimotor cortex stimulation were performed on the same five subjects at both 1.5 and 4T. Four slices covering the motor cortex were acquired. Based on the preliminary experiment on one subject using various postlabeling delays, ΔTI and w were set to 800 ms and 1000 ms in PASL and CASL, respectively, to account for the 5-cm difference in tagging locations between the two methods. The TRs were 3 s and 4 s for PASL and CASL, respectively. In all, 120 acquisitions were performed during the functional scan, leading to a total scan time of 6 min for PASL and 8 min for CASL. The activation paradigm consisted of three cycles of resting periods alternating with activation epochs, i.e., an activation/resting period of 1 min for PASL and 1 min 20 s for CASL. The activation task consisted of bilateral finger tapping paced by a visually presented spot flashing at 2 Hz. The feasibility of whole-brain functional perfusion imaging at 4T was tested on three subjects using 4T PASL with eight slices of coverage. A ΔTI of 1000 ms and TR of 3.4 s were used. The functional scan consisted of 352 acquisitions, with a total scan time of 20 min. Ten cycles of resting/activation periods were carried out, and the activation task consisted of visual stimulation using LED goggles flashing at 10 Hz and simultaneous bilateral self-paced finger tapping.

Data Processing

Data were processed off-line on a Sun Sparc workstation (Sun Micro Systems, Mountain View, CA). For steady-state imaging, the raw images acquired using 4T PASL, 1.5T CASL, and 1.5T PASL were scaled so that the background noise (measured from regions of no signal) was at the same level. Time series of 45 ASL difference images were obtained by pairwise magnitude subtraction between control and labeled images in each scan, followed by averaging to

produce ΔM images. The ΔM signals were measured from whole-brain gray and white matter regions of interest (ROIs) defined from the T_1-weighted anatomical images.

For functional perfusion imaging, the data were motion corrected using a six-parameter, rigid-body, least-squares realignment routine, followed by smoothing in space with a 3D, 5.4-mm FWHM Gaussian kernel. The series of labeled images were shifted in time by one TR using linear interpolation (average of the two adjacent labeled images). Time series of perfusion difference images were generated by pairwise subtraction between the time-matched label and control images. Cross-correlation analysis was used to identify activated voxels, by correlating the time course of perfusion signals with a boxcar reference function using AFNI (27). The significant activation level was arbitrarily set to $P < 0.001$ based on a single subject, corresponding to an absolute correlation coefficient value > 0.4 for the sensorimotor stimulation task and > 0.25 for the simultaneous visual and sensorimotor stimulation task. Individual correlation coefficient activation maps were Talairach normalized based on the T_1-weighted anatomical images, followed by averaging across subjects to produce group activation maps. To evaluate the across-subject variability of activation, a within-region, random-effects analysis was carried out using an unpaired *t*-test on the population of the mean correlation coefficients obtained in the predefined ROIs. The ROIs were defined on the Talairach-normalized T_1-weighted anatomical images which included primary sensorimotor, premotor, and supplementary motor cortex according to Luh et al. (21), and were the same for each individual subject.

RESULTS

Theoretical Calculation

Based on the imaging parameters, theoretical calculation of the ASL perfusion signal as a function of the main field strength is carried out in three steps. The first step is to calculate the fraction of ΔM change with field strength solely due to the T_1 effect. We assume the T_1's of brain tissue, T_{1app}, and blood, T_{1a}, follow approximately a cube root increase with field strength (28), i.e., $T_1 \propto \omega^{0.3}$ where ω is the Larmor frequency of the field. Based on the T_1 values at 1.5T (T_{1app} = 1000 ms, T_{1a} = 1200 ms) (9), the estimated T_1 values at high field match well with the reported experimental results (e.g., T_{1app} = 1240 ms, T_{1a} = 1490 ms at 3T; and T_{1app} = 1350 ms, T_{1a} = 1620 ms at 4T) (29,30). The fraction of ΔM in CASL and PASL as a function of field strength is then calculated according to Eqs. [1] and [3], respectively, and averaged across the assumed values of δ = 1000 ~ 1800 ms (9,23,26), $\Delta TI / w$ = 1000 ~ 1500 ms. We choose to average across multiple different δ and *w* values because the exchange of water spins between blood and brain tissue is more likely to happen during a range of time rather than at a fixed time point, which is very difficult to define, and the delay time also changes in experiments. As displayed in Fig. 1a, the signal increase in the fraction of ΔM due to the T_1 increase as the field changes from 1.5T to 4T is 1.6 times for both PASL and CASL.

As the second step, we calculate the normalized ΔM signal in the ideal case when TE = 0 ms. This is done by

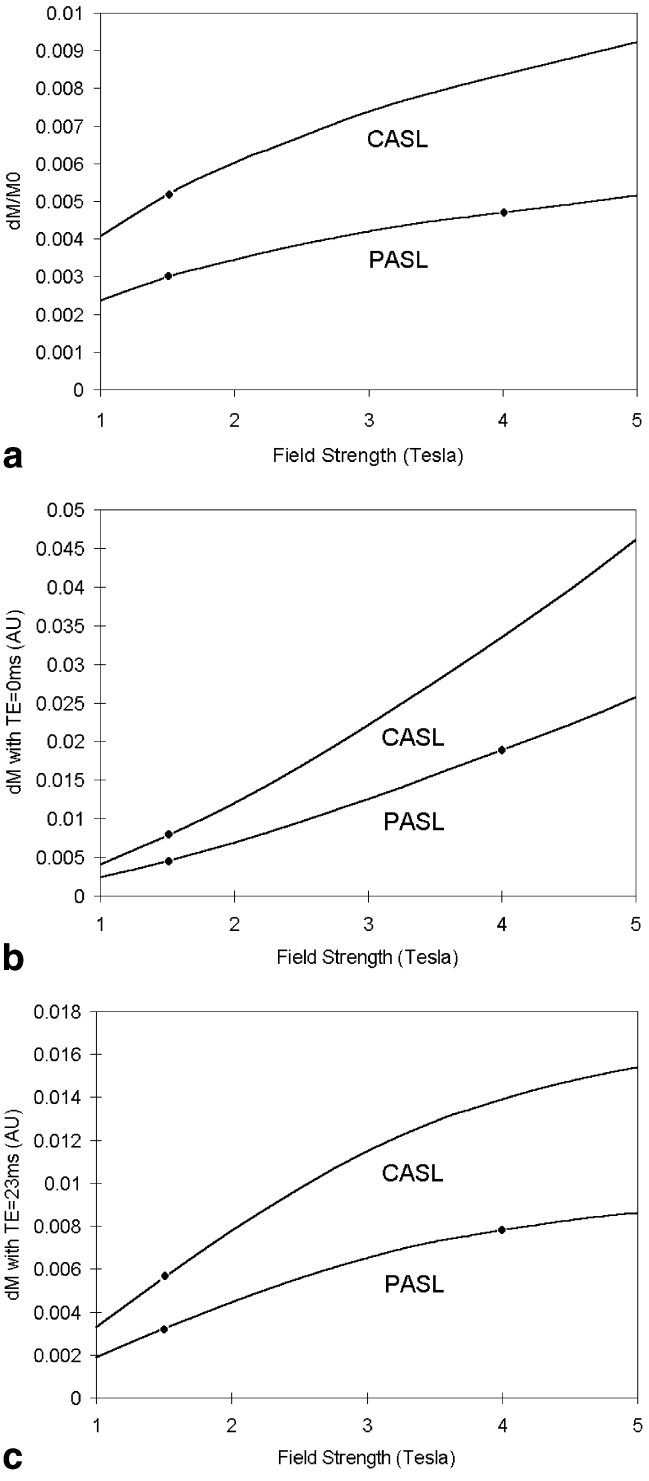

FIG. 1. Theoretical ASL ΔM signal as a function of main field strength, displaying (**a**) fractional ΔM signal change with field strength solely due to T_1 effects, (**b**) normalized ΔM signal change with field strength in the ideal case when TE = 0, and (**c**) realistic estimation of the ΔM signal change with field strength considering the T_2^* effects. The circles indicate the conditions for the experimental data reported.

multiplying the result of step 1 with the intrinsic SNR of M_0, which is proportional to the field strength. The result indicates the theoretical maximum signal gain in ΔM that could be achieved with high field. As displayed in Fig. 1b, 4T PASL and CASL theoretically could yield a 4.2- and 4.3-fold signal gain in ΔM as compared with the same technique at 1.5T, respectively. In the final step, a realistic estimation of the ASL signal as a function of field strength is performed by taking into account the T_2^* effect. Given the fact that the T_2^* of brain is approximately inversely proportional to the field strength, the assumed T_2^* of 70 ms at 1.5T (31) and a TE of 23 ms used in this study, the relative SNR of ΔM acquired using 4T PASL, 1.5T CASL, and 1.5T PASL in our experiment is 2.4:1.7:1. The normalized ΔM signal would be 4.3 if 4T CASL had been carried out (Fig. 1c). As displayed in Fig. 1, the CASL ΔM signal is a factor of 1.7–1.8 higher compared with the PASL ΔM signal, and the ratio between the CASL and PASL ΔM signals tends to increase with field strength.

Equation [1] assumes that no MT effect is presented in the CASL ΔM signal, which is generally true for a multicoil CASL approach. However, MT effect has to be taken into account when a single-coil CASL approach is carried out, as in the present study. The ΔM signal for CASL at 1.5T is therefore calculated according to Eq. [2], with the assumed values of $R_{1ns}/R_{1s} = 0.7$, $R_{1ns} = R_{1app}$ (10), and the predicted relative SNR of ΔM acquired using 4T PASL, 1.5T CASL, and 1.5T PASL in our experiment is 2.4:1.5:1. In all of the above steps, the inversion efficiency, α, is assumed to be 0.98 for PASL (23) and 0.71 for CASL (32), according to the values derived at 1.5T. The possibility of decreased inversion efficiency of the FOCI pulse at high field is estimated by numerical integration of the Bloch equation. A less than 5% decrease in α is found due to the reduced T_2 of blood, and is therefore neglected. The tagging efficiency in CASL with a dual-coil approach at high field could be close to 1 (19); however, the geometry previously employed for this approach generally induces longer arterial transit time. Since these two effects tend to be balanced by each other, it is reasonable to use the same α in CASL for high field.

To compare the sensitivity of the ASL perfusion measurements to errors in T_{1app}, T_{1a}, and δ at different field strengths, the slope of ΔM with respect to these parameters is calculated for ASL techniques at 1.5 and 4T using various values of δ. We choose to vary δ in a relatively large range because it is the most uncertain parameter here. Figure 2 displays the sensitivity of 1.5 and 4T ASL techniques to T_{1app}, T_{1a}, and δ as a function of δ in units of percent change in ΔM per 100 ms error in the corresponding parameter. In general, 4T ASL methods show less sensitivity to the three parameters compared with the same technique at 1.5T, and the sensitivity at 4T per se is less susceptible to δ variations than that at 1.5T. PASL shows less sensitivity to T_{1app} but greater sensitivity to T_{1a} compared with CASL at both 1.5 and 4T, because by the time images are acquired most of the tagged water resides in tissue compartments in CASL vs. vascular compartments in PASL (23). This explanation is supported by the observation that the sensitivity of ASL methods to T_{1app} decreases with δ while the sensitivity to T_{1a} increases with δ, as shown in Fig. 2a and b. In all of the sensitivity

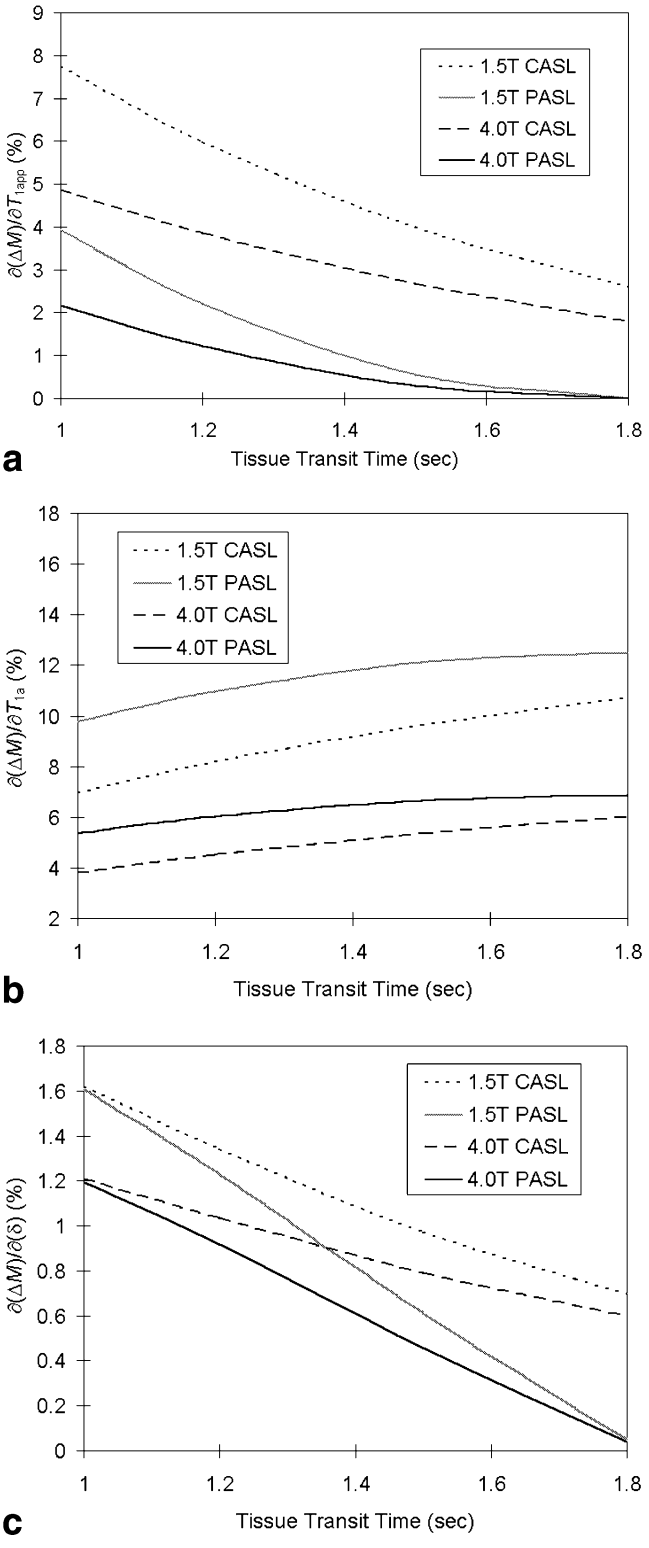

FIG. 2. Sensitivity of ΔM to parameters (**a**) T_{1app}, (**b**) T_{1a}, and (**c**) δ (% change in ΔM per 100 ms change in parameter) as a function of δ for 1.5 and 4T CASL and PASL methods. Assumed values are: $\Delta TI/w$ = 1000 ms, TI_1 = 800 ms, τ = 2000 ms, λ = 0.9 ml/g, T_{1app} = 1000 ms and T_{1a} = 1200 ms at 1.5T, and T_{1app} = 1350 ms and T_{1a} = 1620 ms at 4T.

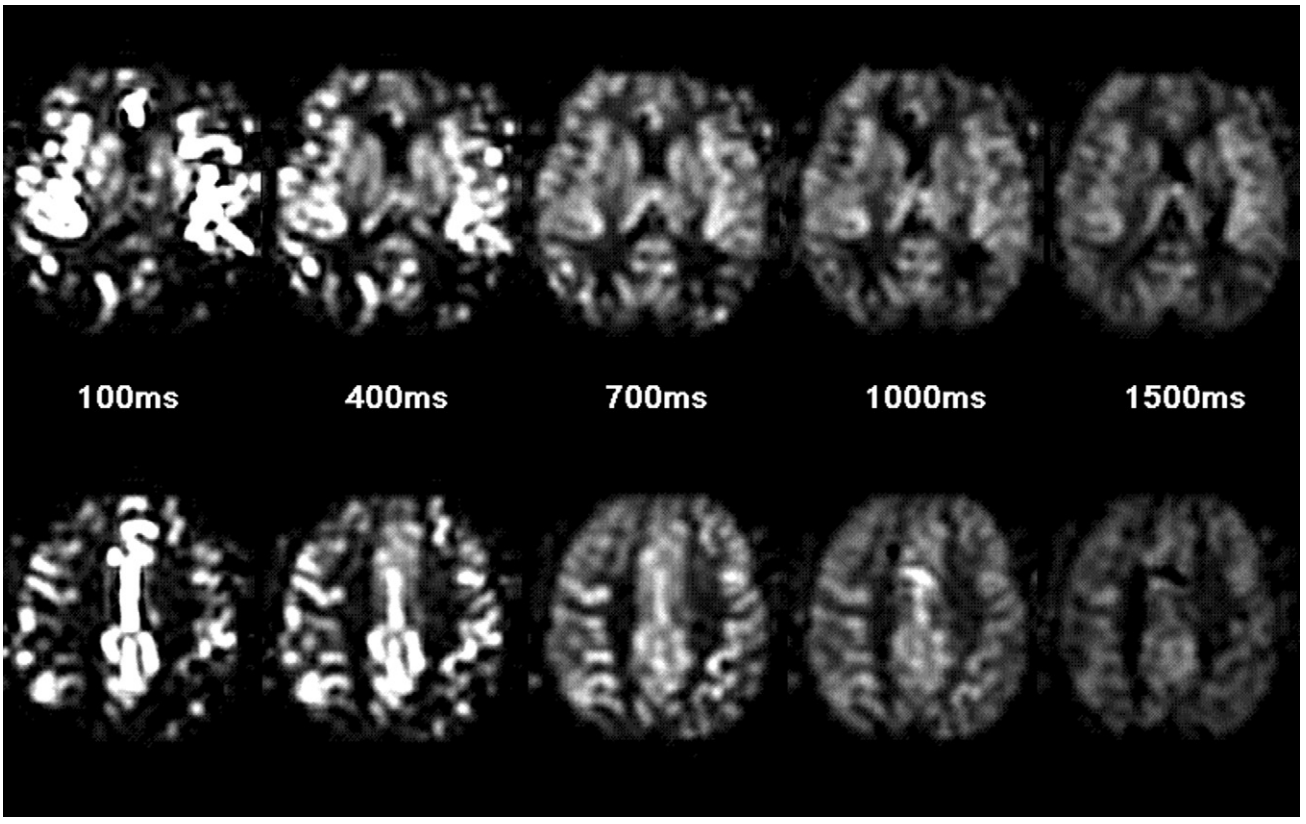

FIG. 3. Effects of postlabeling delay on 4T PASL Δ*M* signals. Two of the eight slices of Δ*M* images from one subject for delays of 100, 400, 700, 1000, and 1500 ms are shown.

calculations, the postlabeling delay is set to 1000 ms. Similar results are obtained with different delay times.

Steady-State Imaging

Figure 3 displays a representative set of difference (Δ*M*) images acquired using 4T PASL with postlabeling delays (ΔTI) from 100 to 1500 ms; two of the eight slices are shown. With ΔTIs longer than 1 s, the bright focal intravascular signals disappear and the cortical structures become manifest. The overall image intensity fades as ΔTI increases due to the T_1 decay of the tagged spins, and cerebrospinal fluid appears dark at all ΔTI values. The spatial pattern and intensity of the Δ*M* images as a function of ΔTI acquired using 4T PASL are consistent with previous tests using various ASL techniques (5,10,26).

Postlabeling delays of 1 s and 1.5 s were used in the steady-state quantitative perfusion imaging for 4T PASL, 1.5T CASL, and 1.5T PASL. Figure 4 displays a representative set of ASL Δ*M* images acquired on one subject using the three approaches. The overall image intensity can be seen to decrease from the inferior to the superior slices in an interleaved manner (1, 3, 5, 7, 2, 4, 6, 8) due to the increased TI caused by the image acquisition order. In terms of image quality, the 4T PASL Δ*M* images provide the best delineation of cortical and subcortical gray matter structures. The deep basal nuclei, including the caudate, putamen, and thalamus, can easily be identified in the 4T images up to the postlabeling delay of 1500 ms. The 4T images have higher intensity in the center regions due to the strong dielectric effects at high field. Both the 1.5T CASL and PASL Δ*M* images appear noisier and show less contrast between the gray and white matter compared with the 4T images. When the Δ*M* images acquired at 1.5T are compared, CASL yields improved image quality compared with PASL, consistent with reported results on comparisons between 1.5T CASL and PASL (23). There are bright focal signals in the 1.5T PASL Δ*M* images, such as the posterior sagittal sinus, attributed to the tagged venous blood flowing superiorly into the imaging slices. These focal signals are rarely seen in the 4T PASL Δ*M* images, probably because the venous blood signal is very small with TE = 23 ms due to the short T_2^* of venous blood at 4T.

Table 1 shows the SNR measured from the whole-brain gray and white matter ROIs along with the calculated contrast-to-noise ratio (CNR) between the gray and white matter, the measured parameters are normalized to the 1.5T PASL values. The ratio of the gray matter SNR of Δ*M* acquired using 4T PASL, 1.5T CASL, and 1.5T PASL is 2.3:1.4:1, a very close match with the theoretical predication of 2.4:1.5:1. In addition to the increased SNR, the 4T images show substantial improvements in the CNR between the gray and white matter, and the ratio of the CNRs acquired using 4T PASL, 1.5T CASL, and PASL is 2.7:1.1:1. Statistical analysis based on a two-tailed paired *t*-test shows that both the SNR and CNR of the 4T PASL data are significantly higher than those of the 1.5T data (see Table 1). The CBF values tabulated in Table 1 are calculated according to Eqs. [2] and [3] with assumed values of

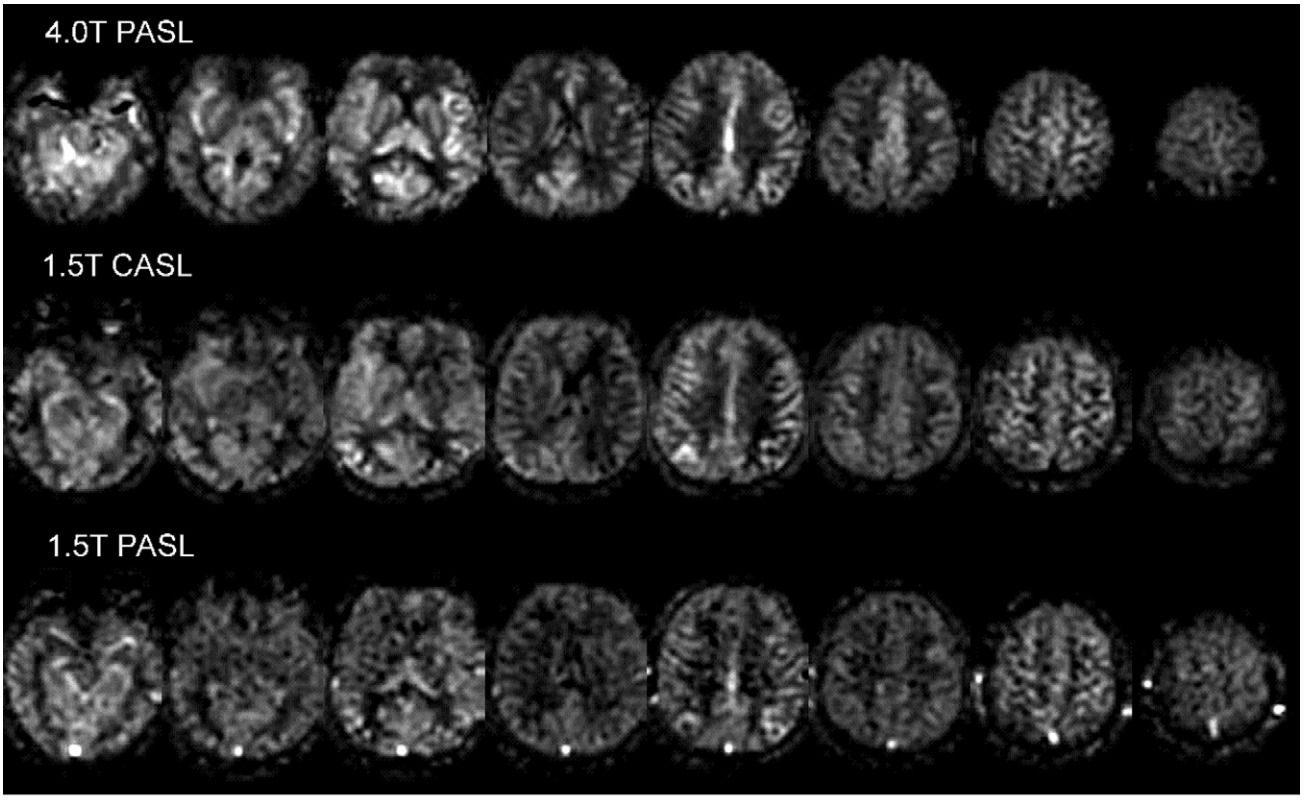

a

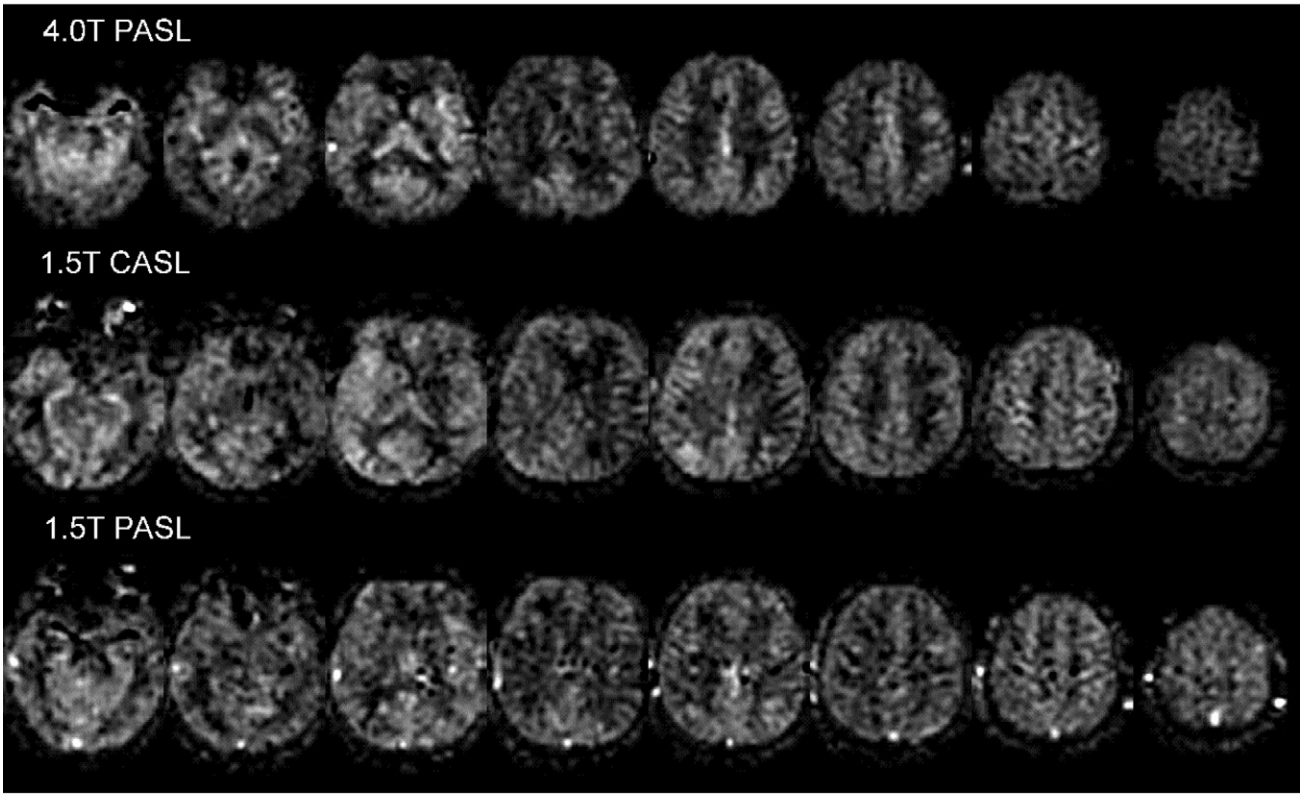

b

FIG. 4. Comparison of the ΔM images acquired using (from the top) 4T PASL, 1.5T CASL, and PASL with the postlabeling delay of (**a**) 1000 ms and (**b**) 1500 ms from one typical subject. Eight slices (8 mm thick, with 2 mm in between) from inferior to superior (left to right) covering most of the brain are shown.

Table 1
Measured Parameters From the Gray and White Matter ROIs in the ASL ΔM Images

		4T PASL	1.5T CASL	1.5T PASL
Delay = 1000 ms	SNR (GM)	2.28 ± 0.41*,††	1.47 ± 0.23†	1.00
	SNR (WM)	1.91 ± 0.43†	1.62 ± 0.30†	1.00
	CNR (GM-WM)	2.54 ± 0.53**,††	1.13 ± 0.26	1.00
	CBF (GM) (ml/100 ml/min)	54.8 ± 9.0	66.8 ± 8.9	63.1 ± 7.5
	CBF (WM) (ml/100 ml/min)	20.1 ± 6.7	28.0 ± 8.0	35.2 ± 4.8
Delay = 1500 ms	SNR (GM)	2.36 ± 0.42*,†	1.33 ± 0.22†	1.00
	SNR (WM)	1.91 ± 0.46†	1.65 ± 0.27†	1.00
	CNR (GM-WM)	2.78 ± 0.56**,††	1.02 ± 0.31	1.00
	CBF (GM) (ml/100 ml/min)	59.2 ± 6.0	70.5 ± 10.9	74.3 ± 12.6
	CBF (WM) (ml/100 ml/min)	20.8 ± 7.7	31.2 ± 6.2	38.5 ± 8.3

SNR and CNR values are normalized to the values acquired using 1.5T PASL.
$^{*}P < 0.05$; $^{**}p < 0.005$ vs. 1.5T CASL (two-tailed t-test), $^{\dagger}P < 0.05$; $^{\dagger\dagger}p < 0.005$ vs. 1.5T PASL (two-tailed t-test).

$\lambda = 0.9$ ml/g and $\delta = 1.5$ s. The values in gray matter (54.8–74.3 ml/100 ml/min) and white matter (20.1–38.5 ml/100 ml/min) are in good agreement with those obtained by positron emission tomography (PET) (33) and various ASL techniques (8–11).

Functional Activation

Figure 5 displays the Talairach-normalized correlation-coefficient activation maps of bilateral finger tapping that are produced by averaging the individual correlation-coefficient activation map across all five subjects. The functional map is superimposed upon transverse sections of Talairach-normalized anatomical images of an individual subject. The same scale is used in the 4T PASL, 1.5T CASL, and PASL images, and is between the average correlation-coefficient values of 0.15 and 0.5 to demonstrate the relative intensity and spatial extent of the activation detected using each of the methods. All three ASL techniques yield robust activation in the bilateral sensorimotor and supplementary motor cortex. The number of activated voxels, average correlation coefficient, and percentage signal change are measured in the predefined ROIs in each subject and are summarized in Table 2. The number of activated voxels detected using 4T PASL is about 14% and 29% more than those detected using 1.5T PASL and 1.5T CASL, respectively. However, this trend of increased numbers of activated voxels at 4T does not reach statistical significance (see Table 2). The postlabeling delay of 1000 ms in CASL, which is 200 ms longer than the delay in PASL, might contribute to the relatively fewer activated

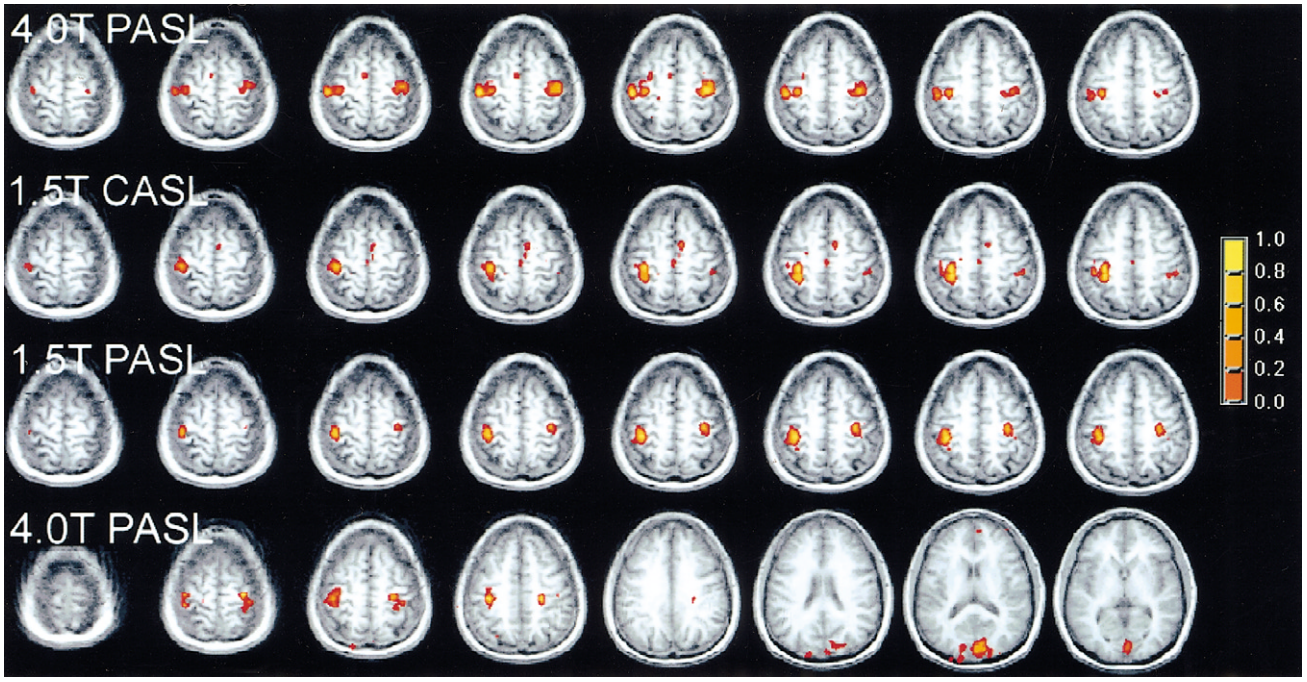

FIG. 5. Comparison of the Talairach-normalized and averaged ($N = 5$) correlation-coefficient activation maps of bilateral finger tapping acquired using 4T PASL, 1.5T CASL, and 1.5T PASL (the upper three panels). The scale (from 0 to 1) is normalized between the average correlation-coefficient values of 0.15 and 0.5. Talairach-normalized and averaged ($N = 3$) activation maps of simultaneous visual and motor cortex activation acquired using 4T PASL are displayed in the bottom panel. The scale is normalized between the averaged correlation-coefficient values of 0.12 and 0.4.

Table 2
Number of Activated Voxels, Average Correlation Coefficient and Signal Change, Along With the T-value Associate With the Random-Effects Across-Subject Test

	4T PASL	1.5T CASL	1.5T PASL
Number of activated voxels	66.0 ± 46.5	51.2 ± 21.9	58.2 ± 38.1
Average correlation coefficient	0.441 ± 0.050	0.449 ± 0.027	0.442 ± 0.030
Average percentage signal change (%)	46.4 ± 17.8*	67.6 ± 9.7	90.9 ± 17.4
T score Across subject	2.09	5.04	3.47

*$P < 0.005$ vs. 1.5T PASL (two-tailed t-test).

voxels in the CASL data. The average correlation coefficients in the three data sets are not significantly different from each other. The *t*-value associated with the random-effects, across-subject test of the correlation coefficient acquired using 4T PASL is lower than the *t*-values of the 1.5T PASL and 1.5T CASL data, suggesting more robust results across-subject at 1.5T than 4T. Due to the small sample size ($N = 5$), a general implication with respect to the relative across-subject variability of ASL methods at 1.5 and 4T would require more data sets. To avoid the effects of arbitrary threshold, data analysis was also carried out using different threshold levels in individual subjects, and similar results were obtained.

An interesting finding in our experiment is that the mean fractional perfusion signal increase induced by finger tapping was higher in the 1.5T PASL (90.9%) and 1.5T CASL data (67.6%) than in the 4T PASL (46.4%) data. Statistical analysis indicates that the difference between the 1.5 and 4T PASL data is highly significant (see Table 2), while the difference between the 1.5T CASL and 4T PASL data barely achieves significance ($P = 0.06$). The high percentage signal changes in our 1.5T ASL data are consistent with reported values (around 100%) in ASL studies on motor cortex activation at 1.5T (34). Meanwhile, a fractional signal increase of 20–50% seems consistent with the findings from PET studies on motor cortex stimulation (35). The reason for the difference in signal changes at 1.5 and 4T is not well understood, and will be discussed below. The feasibility of whole-brain perfusion fMRI using 4T PASL is demonstrated by simultaneous visual and motor cortex activation, as displayed in Fig. 5 of the Talairach-normalized correlation-coefficient activation maps averaged across three subjects. Robust and consistent activation in the visual and sensorimotor cortex is observed in each of the three subjects.

DISCUSSION

Benefits of High-Field ASL

The results presented above demonstrate the feasibility and benefits of multislice high-field perfusion imaging using ASL approaches. The SNR of the gray matter signal in the 4T PASL ΔM images is a factor of 1.6 and 2.3 higher than the SNR measured in the 1.5T CASL and 1.5T PASL images, respectively. The CNR between the gray and white matter in the 4T ΔM images is approximately a factor of 2.7 higher than the CNR in the 1.5T ΔM images. Theoretical calculation indicates that 4T ASL approaches are less sensitive to errors in the T_1's of brain tissue and blood, as well as in tissue transit time.

The close match between the experimental results and theoretical predictions of the ΔM signals at 1.5 and 4T validates the theoretical model (Fig. 1) for the dependence of ASL signal on the main field strength. As an inference of the theoretical model, image acquisition sequences with short TE are highly advantageous in ASL approaches in terms of maximizing the SNR gain at high field. Gradient-echo SPIRAL and half-*k*-space EPI methods acquire data from the center of the *k*-space and have an effective TE of a few milliseconds. An approximately 50% improvement in the SNR gain at 4T could be achieved if the current gradient-echo EPI approach were to be replaced by these acquisition methods. Another inference from the predicted function is that CASL would be more advantageous than PASL at high field if it could be carried out with a multicoil or special single-coil approach, e.g., 4T CASL could yield about 4–5 times SNR compared with 1.5T ASL approaches.

Susceptibility Effects

Apart from the advantages described above, one major limitation at high field is greater susceptibility effects, which lead to signal loss and distortion in brain regions with high static field inhomogeneity. In order to avoid deterioration of the ASL image quality, shortened TEs and acquisition windows are highly preferable at high field. As mentioned, acquisition methods with efficient *k*-space trajectories, such as SPIRAL and half-*k*-space EPI, have very short TEs and acquisition windows, and are advantageous in minimizing the susceptibility effects while maximizing the SNR gain at high field. In addition, spin-echo approaches can be used in combination with these methods to further reduce the susceptibility effects. In the current study, when identical acquisition methodologies were used at both 1.5 and 4T, lower effective in-plane resolution and stronger signal loss in the orbital frontal cortex and inferior temporal lobe were observed in the 4T images (Fig. 4) compared with the 1.5T images.

The greater susceptibility effects at high field may also contribute to the reduced fractional perfusion signal change during motor activation at 4T. When the blood flow increases due to neural activation, a portion of the additional labeled water may not be fully extracted, and instead may pass on into the veins. While the T_2^* of venous blood and brain is not very different at 1.5T, the T_2^* of venous blood becomes very short due to the strong susceptibility effects of deoxyhemoglobin at 4T, rendering the unextracted labeled water invisible with the current TE of 23 ms (36) (see Fig. 4). This speculation is supported by a recent study which indicated that more tagged spins exit the capillary bed without passing into the tissue when blood flow increases (37). If this explanation is correct,

roughly half of the increased blood water associated with regional brain activation would not have passed into the brain tissue, based on the observed changes at 1.5 and 4T using the PASL approach. This suggests that the current perfusion model, which neglects the clearance of the tag by outflow, might not be accurate during brain activation.

Physiological Noise

Another important factor in high-field ASL is physiological noise, including metabolic fluctuations, tissue motion, and pulsation. The physiological noise level may increase with static field strength (38) and may be the dominating factor in determining the sensitivity of ASL perfusion imaging to functional activation. The measurements of SNR and CNR employed in the present study primarily reflect effects of scanner noise. To evaluate the physiological noise level at 1.5 and 4T, we also measured the temporal stability of the time series of the difference perfusion images acquired during resting state. Based on the histogram of the normalized temporal standard deviation (SD), determined by the SD divided by the mean of the time course of the ΔM images in each voxel of the brain, the ratio of the relative mean normalized temporal SD acquired using 4T PASL, 1.5T CASL, and 1.5T PASL is 0.84:0.90:1.00. The mean normalized temporal SD of the 4T PASL data is significantly lower than the 1.5T PASL data ($P < 0.05$), but not significantly different from the 1.5T CASL data. The improvement in temporal stability as the field changes from 1.5 to 4T is compromised compared with the substantial improvement in the SNR and CNR, suggesting greater physiological noise at 4T. When the above temporal stability analysis was carried out on the average time course of the ΔM images in the whole-brain gray matter ROI, the ratio of the relative normalized temporal SD acquired using 4T PASL, 1.5T CASL, and 1.5T PASL became 1.08:0.56:1.00. The values of the 1.5 and 4T PASL data are significantly higher than that of the 1.5T CASL data ($P < 0.05$). This further decreased temporal stability within a large ROI suggests the presence of spatially coherent noise which cannot be suppressed by spatial averaging—for example, noise consisting of cardiac or respiratory pulsation (39). This effect of physiological noise, together with the higher apparent ASL signal change in response to motor cortex stimulation at 1.5T, likely accounts for the similar number of activated voxels and mean correlation coefficient as well as the greater intersubject variability in the 4T functional data as compared with the 1.5T functional data.

While the ratio of the signal to thermal noise can only be improved by increasing field strength, assuming the coil is optimal, the contribution of physiological noise to the measurement of flow may be reduced if the underlying sources and mechanisms can be understood. It has been reported that the magnitude of brain physiological noise, the primary source of physiological noise at high field, is proportional to the TE and raw image intensity, resulting in the maximum noise magnitude at TE = T_2^* and the minimum at TE = 0 (38). The aforementioned short TE acquisition methods will also be preferable in alleviating the effects of brain physiological noise. In addition, physiological noise due to pulsation can be effectively minimized by cardiac or respiratory gating (39). Since a large portion of the physiological noise is spatially coherent, the global mean time course of the image intensity can also be included in the regression analysis as a covariant to account for the noise, an approach we are currently investigating. Based on the improved temporal stability in the CASL data compared with the PASL data at 1.5T, high-field CASL approaches should also be preferable in terms of reducing the physiological noise. This improvement in temporal stability will be smaller than the improvement in SNR, primarily because the CASL raw image intensity is higher than the PASL raw image signal, which is usually not fully relaxed. Background suppression approaches would also reduce the physiological noise by suppressing the static raw image signal (40). However, to implement this approach at high field, special care must be taken to limit the RF deposition of multiple inversions required in the background suppression technique.

ACKNOWLEDGMENTS

This research was supported by NIH grants HD39621 (to J.A.D.) and AG19599 (to D.C.A.); and an unrestricted grant from GE Medical Systems (to M.D.S.). The authors thank Dr. Hee Kwon Song for help with the numerical integration of the Bloch equation, and Dr. Daniel Kimberg for assistance with the statistical analysis of the functional data.

APPENDIX

The present theoretical calculation is based on the two-compartment perfusion model (10), in which the observed ΔM signal consists of signals from tissue and arterial vascular compartments. An important variable missing from the original CASL model was the duration of labeling, which was assumed to be infinitely long. By replacing $-\infty$ in eq. 15 of Ref. 10 with the time the tagging bolus first arrives in the tissue compartment, $\delta - \tau - w$, the tissue ΔM signal is given by (assuming the imaging time is 0):

$$\Delta M_{tissue} = \frac{-2M_0 f\alpha}{\lambda} \exp(-\delta R_{1a}) \int_{\delta-\tau-w}^{\min(\delta-w,0)} dt \exp(tR_{1app})$$

$$= \frac{-2M_0 f\alpha}{\lambda R_{1app}} \exp(-\delta R_{1a}) \qquad \tau + w > \delta$$

$$\times [\exp(\min(\delta - w,0)R_{1app})$$

$$- \exp((\delta - \tau - w)R_{1app})]$$

$$\Delta M_{tissue} = 0 \qquad \tau + w < \delta. \quad [A1]$$

Based on eq. 20 of Ref. 10, the arterial signal is given by the difference signal between the inflow and outflow of the arterial vascular compartment, which are acquired by integrating the modified Bloch equation (1) from $\delta_a - \tau - w$ to 0 and from $\delta - \tau - w$ to 0, respectively. If no tagged blood water has arrived in the tissue compartment by the time image is acquired ($\tau + w < \delta$), all the labeled blood will stay in the arterial vascular compartment (no outflow).

$$\Delta M_{arterial} = \frac{-2M_0 f\alpha}{\lambda}\left(\int_{\delta_a-\tau-w}^{\min(\delta_a-w,0)} dt\,\exp((t-\delta_a)R_{1a}) - \int_{\delta-\tau-w}^{\min(\delta-w,0)} dt\,\exp((t-\delta)R_{1a})\right) \qquad \tau + w > \delta$$

$$= \frac{-2M_0 f\alpha}{\lambda R_{1a}}\left[\exp((\min(\delta_a - w,0) - \delta_a)R_{1a}) - \exp((\min(\delta - w,0) - \delta)R_{1a})\right]$$

$$\Delta M_{arterial} = \frac{-2M_0 f\alpha}{\lambda}\left(\int_{\delta_a-\tau-w}^{\min(\delta_a-w,0)} dt\,\exp((t-\delta_a)R_{1a})\right) \qquad \tau + w < \delta$$

$$= \frac{-2M_0 f\alpha}{\lambda R_{1a}}\left[\exp((\min(\delta_a - w,0) - \delta_a)R_{1a}) - \exp(-(\tau + w)R_{1a})\right] \qquad [A2]$$

Equation [1] is simply the sum of the above two equations. In the presence of MT effects, $R_{1\mathrm{app}}$ is equal to $R_{1\mathrm{s}}$ during the tagging pulse and to $R_{1\mathrm{ns}}$ afterwards. The tissue signal is then calculated by

$$\Delta M_{tissue} = \frac{-2M_0 f\alpha}{\lambda}\exp(-\delta R_{1a})\left(\exp(-wR_{1ns})\int_{\min(\delta-\tau,0)}^{0} dt\,\exp(tR_{1s}) + \int_{-w}^{\min(\delta-w,0)} dt\,\exp(tR_{lns})\right)$$

$$= \frac{-2M_0 f\alpha}{\lambda}\exp(-\delta R_{1a})\left\{\begin{array}{l}\dfrac{\exp(-wR_{lns})}{R_{ls}}[1 - \exp(\min(\delta - \tau,0)R_{ls})] + \\ \dfrac{1}{R_{lns}}[\exp(\min(\delta - w,0)R_{lns}) - \exp(-wR_{lns})]\end{array}\right\} \qquad \tau + w > \delta$$

$$\Delta M_{tissue} = 0 \qquad \tau + w < \delta \qquad [A3]$$

Equation [2] is simply the sum of Eqs. [A2] and [A3].

For PASL, the tissue signal is given by (eq. 22 in Ref. 11)

$$\Delta M_{tissue} = \frac{-2M_0 f\alpha}{\lambda}\exp(-TI_2 R_{1a})\int_{\delta-TI_2}^{\min(\delta+\tau-TI_2,0)} dt\,\exp(t\Delta R) \qquad TI_2 > \delta$$

$$= \frac{-2M_0 f\alpha}{\lambda}\exp(-TI_2 R_{1app})[\exp(\min(TI_2,\delta + TI_1)\Delta R) - \exp(\delta\Delta R)]/\Delta R$$

$$\Delta M_{tissue} = 0 \qquad TI_2 < \delta \qquad [A4]$$

Similar to CASL, the arterial signal in PASL is given by the difference signal between the inflow and outflow of the arterial vascular compartment, which are acquired by integrating the modified Bloch equation from $\delta_a - TI_2$ to 0, and from $\delta - TI_2$ to 0, respectively. If no tagged blood water has arrived in the tissue compartment by the time image is acquired ($TI_2 < \delta$), all the labeled blood will stay in the arterial vascular compartment (no outflow).

$$\Delta M_{arterial} = \frac{-2M_0 f\alpha}{\lambda} \exp(-TI_2 R_{1a}) \left(\int_{\delta_a - TI_2}^{\min(\delta_a - \Delta TI, 0)} dt - \int_{\delta - TI_2}^{\min(\delta - \Delta T1, 0)} dt \right) \qquad TI_2 > \delta$$

$$= \frac{-2M_0 f\alpha}{\lambda} \exp(-TI_2 R_{1a}) [(\min(\delta_a - \Delta TI, 0) - \delta_a) - (\min(\delta - \Delta TI, 0) - \delta)]$$

$$\Delta M_{arterial} = \frac{-2M_0 f\alpha}{\lambda} \exp(-TI_2 R_{1a}) \left(\int_{\delta_a - TI_2}^{\min(\delta_a - \Delta TI, 0)} dt \right) \qquad TI_2 < \delta$$

$$= \frac{-2M_0 f\alpha}{\lambda} \exp(-TI_2 R_{1a}) [\min(\delta_a - \Delta TI, 0) - (\delta_a - TI_2)] \qquad [A5]$$

Equation [3] is simply the sum of Eqs. [A4] and [A5]. In all of the above deductions, the delay time, w/ΔTI, is assumed to be greater than the arterial transit time, δ_a.

REFERENCES

1. Detre JA, Leigh JS, Williams DS, Koretsky AP. Perfusion imaging. Magn Reson Med 1992;23:37–45.
2. Williams DS, Detre JA, Leigh JS, Koretsky AP. Magnetic resonance imaging of perfusion using spin inversion of arterial water. Proc Natl Acad Sci USA 1992;89:212–216.
3. Detre JA, Alsop DC. Perfusion fMRI with arterial spin labeling (ASL). In: Moonen CTW, Bandettini PA, editors. Functional MRI. Heidelberg: Springer; 1999. p 47–62.
4. Wong EC. Potential and pitfalls of arterial spin labeling based perfusion imaging techniques for MRI. In: Moonen CTW, Bandettini PA, editors. Functional MRI. Heidelberg: Springer; 1999. p 63–69.
5. Edelman RR, Siewert B, Darby DG, Thangaraj V, Nobre AC, Mesulam MM, Warach S. Qualitative mapping of cerebral blood flow and functional localization with echo-planar MR imaging and signal targeting with alternating radio frequency. Radiology 1994;192:513–520.
6. Kwong KK, Chesler DA, Weisskoff RM, Donahue KM, Davis TL, Ostergaard L, Campbell TA, Rosen BR. MR perfusion studies with T1-weighted echo planar imaging. Magn Reson Med 1995;34:878–887.
7. Kim SG. Quantification of relative cerebral blood flow change by flow-sensitive alternating inversion recovery (FAIR) technique: application to functional mapping. Magn Reson Med 1995;34:293–301.
8. Yang Y, Frank JA, Hou L, Ye FQ, McLaughlin AC, Duyn JH. Multislice imaging of quantitative cerebral perfusion with pulsed arterial spin labeling. Magn Reson Med 1998;39:825–832.
9. Ye FQ, Mattay VS, Jezzard P, Frank JA, Weinberger DR, McLaughlin AC. Correction for vascular artifacts in cerebral blood flow values measured by using arterial spin tagging techniques. Magn Reson Med 1997;37:226–235.
10. Alsop DC, Detre JA. Reduced transit-time sensitivity in noninvasive magnetic resonance imaging of human cerebral blood flow. J Cereb Blood Flow Metab 1996;16:1236–1249.
11. Wong EC, Buxton RB, Frank LR. Quantitative imaging of perfusion using a single subtraction (QUIPSS and QUIPSS II). Magn Reson Med 1998;39:702–708.
12. Detre JA, Alsop DC, Vives LR, Maccotta L, Teener JW, Raps EC. Noninvasive MRI evaluation of cerebral blood flow in cerebrovascular disease. Neurology 1998;50:633–641.
13. Alsop DC, Detre JA, Grossman M. Assessment of cerebral blood flow in Alzheimer's disease by spin-labeled magnetic resonance imaging. Ann Neurol 2000;47:93–100.
14. Chalela JA, Alsop DC, Gonzalez-Atavalez JB, Maldjian JA, Kasner SE, Detre JA. Magnetic resonance perfusion imaging in acute ischemic stroke using continuous arterial spin labeling. Stroke 2000;31:680–687.
15. Aguirre GK, Detre JA, Zarahn E, Alsop DC. Experimental design and the relative sensitivity of BOLD and perfusion fMRI. Neuroimage 2002;15:488–500.
16. Crelier GR, Hoge RD, Munger P, Pike GB. Perfusion-based functional magnetic resonance imaging with single-shot RARE and GRASE acquisitions. Magn Reson Med 1999;41:132–136.
17. Liu HL, Kochunov P, Hou J, Pu Y, Mahankali S, Feng CM, Yee SH, Wan YL, Fox PT, Gao JH. Perfusion-weighted imaging of interictal hypoperfusion in temporal lobe epilepsy using FAIR-HASTE: comparison with H(2)(15)O PET measurements. Magn Reson Med 2001;45:431–435.
18. Chen Q, Siewert B, Bly BM, Warach S, Edelman RR. STAR-HASTE: perfusion imaging without magnetic susceptibility artifact. Magn Reson Med 1997;38:404–408.
19. Zaharchuk G, Ledden PJ, Kwong KK, Reese TG, Rosen BR, Wald LL. Multislice perfusion and perfusion territory imaging in humans with separate label and image coils. Magn Reson Med 1999;41:1093–1098.
20. Alsop DA. Improved efficiency for multi-slice continuous arterial spin labeling using time varying gradients. In: Proceedings of the 9th Annual Meeting of ISMRM, Glasgow, Scotland, 2001. p 1562.
21. Luh WM, Wong EC, Bandettini PA, Ward BD, Hyde JS. Comparison of simultaneously measured perfusion and BOLD signal increases during brain activation with T(1)-based tissue identification. Magn Reson Med 2000;44:137–143.
22. Yongbi MN, Yang Y, Frank JA, Duyn JH. Multislice perfusion imaging in human brain using the C-FOCI inversion pulse: comparison with hyperbolic secant. Magn Reson Med 1999;42:1098–1105.
23. Wong EC, Buxton RB, Frank LR. A theoretical and experimental comparison of continuous and pulsed arterial spin labeling techniques for quantitative perfusion imaging. Magn Reson Med 1998;40:348–355.
24. Wang J, Jahng GH, Lai S. Multislice online quantitative perfusion imaging using FAIR exempting separate T1 measurement (FAIREST). In: Proceedings of the 9th Annual Meeting of ISMRM, Glasgow, Scotland, 2001. p 1561.
25. Alsop DC, Detre JA. Multisection cerebral blood flow MR imaging with continuous arterial spin labeling. Radiology 1998;208:410–416.
26. Gonzalez-At JB, Alsop DC, Detre JA. Perfusion and transit time changes during task activation determined with steady-state arterial spin labeling. Magn Reson Med 2000;43:739–746.
27. Cox RB. AFNI: software for analysis and visualization of functional magnetic resonance neuroimages. Comput Biomed Res 1996;29:162–173.
28. Bottomley PA, Hardy CJ, Argersinger RE, Allen-Moore G. A review of 1H nuclear magnetic resonance relaxation in pathology: are T1 and T2 diagnostic? Med Phys 1987;14:1–37.
29. Kim SG, Hu X, Ugurbil K. Accurate T1 determination from inversion recovery images: application to human brain at 4 Tesla. Magn Reson Med 1994;31:445–449.
30. Wansapura JP, Holland SK, Dunn RS, Ball WS. 3.0 Tesla study of NMR relaxation times in the human brain. In: Proceedings of the 3rd Annual Meeting of SMR, Nice, France, 1995. p 685.

31. Yang Y, Wen H, Mattay VS, Balaban RS, Frank JA, Duyn JH. Comparison of 3D BOLD functional MRI with spiral acquisition at 1.5 and 4.0 T. Neuroimage 1999;9:446–451.
32. Alsop DC, Detre JA. Multisection cerebral blood flow MR imaging with continuous arterial spin labeling. Radiology 1998;208:410–416.
33. Leenders KL, Perani D, Lammertsma AA, Heather JD, Buckingham P, Healy MJ, Gibbs JM, Wise RJ, Hatazawa J, Herold S, Beany PR, Brooks DJ, Spinks T, Rhodes G, Fracowiak RS, Jones T. Cerebral blood flow, blood volume and oxygen utilization. Normal values and effect of age. Brain 1990;113:27–47.
34. Buxton RB, Frank LR, Wong EC, Siewert B, Warach S, Edelman RR. A general kinetic model for quantitative perfusion imaging with arterial spin labeling. Magn Reson Med 1998;40:383–396.
35. Colebatch JG, Deiber MP, Passingham RE, Friston KJ, Frackowiak RS. Regional cerebral blood flow during voluntary arm and hand movements in human subjects. J Neurophysiol 1991;65:1392–1401.
36. Menon RS, Ogawa S, Tank DW, Ugurbil K. 4 Tesla gradient recalled echo characteristics of photic stimulation-induced signal changes in the human primary visual cortex. Magn Reson Med 1993;30:380–386.
37. Ewing JR, Cao Y, Fenstermacher J. Single-coil arterial spin-tagging for estimating cerebral blood flow as viewed from the capillary: relative contributions of intra- and extravascular signal. Magn Reson Med 2001; 46:465–475.
38. Krueger G, Kastrup A, Glover GH. Neuroimaging at 1.5T and 3.0T: comparison of oxygenation-sensitive magnetic resonance imaging. Magn Reson Med 2001;45:595–604.
39. Jezzard P. Physiological noise: strategies for correction. In: Moonen CTW, Bandettini PA, editors. Functional MRI. Heidelberg: Springer; 1999. p 173–182.
40. Ye FQ, Frank JA, Weinberger DR, McLaughlin AC. Noise reduction in 3D perfusion imaging by attenuating the static signal in arterial spin tagging (ASSIST). Magn Reson Med 2000;44:92–100.